Polym. Bull. (2013) 70:2451–2470
DOI 10.1007/s00289-013-0966-4

ORIGINAL PAPER

Synthesis of *kappa*-carrageenan-g-poly(acrylamide)/ sepiolite nanocomposite hydrogels and adsorption of cationic dye

Gholam Reza Mahdavinia · Adeleh Asgari

Received: 25 January 2013 / Accepted: 22 April 2013 / Published online: 6 June 2013

Abstract In this study, nanocomposite hydrogels from grafting of acrylamide onto *kappa*-carrageenan biopolymer were prepared in the presence of sepiolite clay. Methylenebisacrylamide and ammonium persulfate were used as cross-linker and initiator, respectively. The sepiolite nanoclay was introduced into hydrogel matrix without any chemical treatment. The structure of nanocomposites was investigated by FTIR, SEM, TEM, and TGA techniques. The TEM image showed that sepiolite exists as individual needle's shape. The swelling of hydrogels were studied in distilled water, salt solutions, and various pHs. The obtained nanocomposites were evaluated to remove of cationic crystal violet (CV) dye from water. The kinetic and isotherm of adsorption of dye onto nanocomposites were studied and analyzed according to kinetic and isotherm models. The results showed that the pseudo-second-order adsorption kinetic was predominated for the adsorption of CV onto nanocomposites. The experimental equilibrated adsorption capacity of nanocomposites was analyzed using Freundlich and Langmuir isotherm models. The results corroborated that the experimental data fit the Langmuir isotherm the best. By varying the pH of initial dye solution, while the clay-free hydrogel showed relatively pH-independent adsorption behavior, the nanocomposites depicted pH-dependent adsorption.

Keywords *kappa*-Carrageenan · Sepiolite · Nanocomposite · Hydrogel · Adsorption

G. R. Mahdavinia (✉) · A. Asgari
Department of Chemistry, Faculty of Science, University of Maragheh,
55181-83111 Maragheh, Iran
e-mail: gholamreza.mahdavinia@gmail.com

Introduction

Hydrogels are cross-linked hydrophilic polymers that can absorb considerable amount of water and aqueous fluid [1]. Based on sources of initial materials to synthesize hydrogels, they can be classified into bio- or synthetic-based hydrogels [2]. Because of biodegradability and biocompatibility of biopolymers, the hydrogels from biopolymers have attracted the attention of scientist. Hydrogels from biopolymers such as chitosan, cellulose, carrageenan, alginate, collagen, and modified biopolymers have been synthesized and studied [3–9]. Bio-based hydrogels are also found to be valuable in some specialized applications including controlled delivery of bioactive agents [10] and wastewater treatment [11].

Industry is a huge source of water pollution; it produces pollutants that are excessively harmful to people and the environment. Colored water and solutions containing toxic heavy metals from many industries such as dye, textile, paper, plastic, plating, and mining facilities produce considerable polluted waters. The pollutions must be removed from wastewater before discharging it into the environment. Coagulants, oxidizing agents, ultrafiltration, electrochemical, and adsorption techniques have been applied to remove dyes from aqueous solutions [12]. Because of cost-effective and ease of operation, the adsorption method has been spread. The ionic types of hydrogels comprise anionic ($-CO_2^-$, $-SO_3^-$) or cationic pendants ($-NR_3^+$) [13]. The presence of these ionic groups in the hydrogels opens potential area of application that is related to remove pollutants from wastewaters [14].

Recent advancements in water treatments have led to the introducing of nanoclays with the high surface area into hydrogel matrix to improve the both adsorption rate and capacity [15]. Sodium montmorillonite, laponite, sepiolite, attapulgite, and bentonite are the classes of nanoclays that on inclusion into hydrogels have improved the dye adsorption behavior of these materials [16–20].

Carrageenan is a collective term for linear sulfated polysaccharides produced by alkaline extraction from red seaweed. The repeat unites the *kappa*-carrageenan were shown in Fig. 1. Because of their exceptional properties, carrageenans are broadly used as ingredients in a variety of applications. Since carrageenan is a highly negatively charged polysaccharide, it can interact with species carrying a positive charge. While many reports are published in this regard, such as interaction of carrageenan with univalent and divalent cations [21], with gelatin [22] and with chitosan [23], the removal of cationic dyes from water has not widely studied using this biopolymer.

In our previous works, we attempt to synthesize and evaluate nanocomposite hydrogels based on *kappa*-carrageenan using sodium montmorillonite and laponite RD nanoclays [24–26]. In this study, we tried to investigate the nanocomposite hydrogels from *kappa*-carrageenan in the presence of sepiolite nanoclay. The effect of sepiolite on the removal of crystal violet dye from water was evaluated.

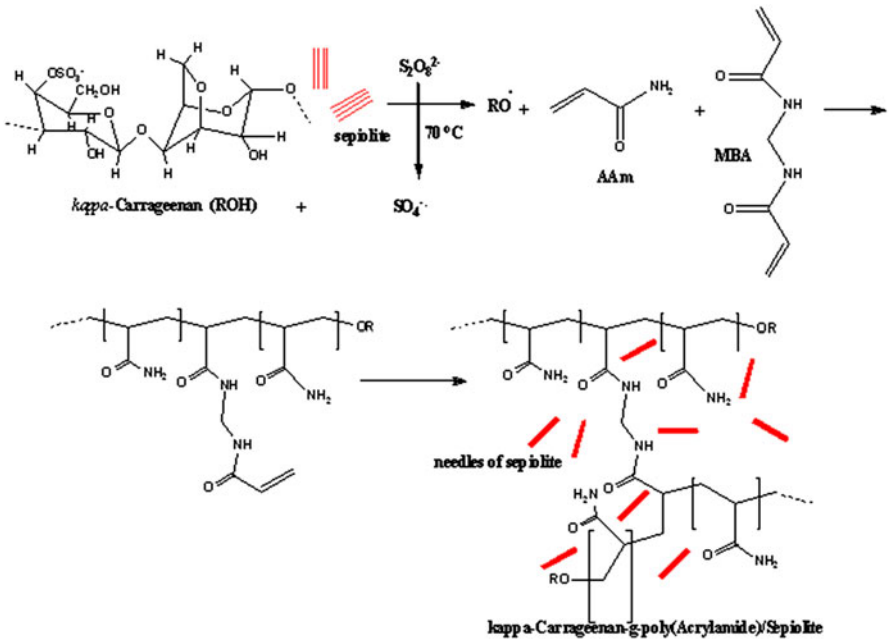

Fig. 1 A simple scheme for synthesis of carrageenan-based nanocomposite hydrogel

Experimental

Materials

kappa-Carrageenan was obtained from Condinson Co., Denmark and used without any purification. Sepiolite (TOLSA, Spain) was used as received. Raw sepiolite composed of 51.95 % SiO_2, 2.14 % Al_2O_3, 0.41 % Fe_2O_3, 2.77 % CaO, 23.35 % MgO, 0.22 % Na_2O, 0.36 % K_2O, 0.08 % TiO_2, and 0.52 % SO_3 was used without any chemical treatment. Acrylamide (AAm) was purchased from Nalco Chemical Co., the Netherlands. It was used after recrystallization from acetone. *N*,*N*-methylenebisacrylamide (MBA) was purchased from Fluka and ceric ammonium nitrate from Merck. Other chemicals were analytical and were used as received.

Synthesis of nanocomposite hydrogels

In typical experiments, different amount of sepiolite clay (0, 0.22, and 0.46 g) were dispersed into 30 mL of distilled water and stirred overnight. The dispersed clay was sonicated for 30 min. Then, 1 g of *kappa*-carrageenan was added to the solution and the temperature of reactor was adjusted at 70 °C. After complete dissolution of *kappa*-carrageenan, the dissolved oxygen was removed using N_2 gas for 30 min. The ammonium persulfate initiator (dissolved in 2 mL water) was added and allowed to induce free radicals onto *kappa*-carrageenan for 5 min. Finally, 3 g of

acrylamide and 0.1 g of MBA (dissolved in 2 mL water) were poured into polymerization solution. The produced nanocomposites were cut into small pieces and immersed in excess water to extract the unreacted components. After purification of nanocomposites for 2 days, the samples were dried at 50 °C for constant weight. The dried samples were ground and passed through a 40-mesh sieve to achieve uniform particle size. The samples were kept away from light and moisture. The H, NH5, and NH10 in the text and figures are the clay-free hydrogel and hydrogels containing 0.22 and 0.46 g of sepiolite, respectively.

Swelling measurements

Nanocomposite hydrogel samples (0.10 g) were immersed in 100 ml distilled water and allowed to soak for 24 h at room temperature. After this time, they were removed from the water, blotted with filter paper to remove surface water, weighed, and the DS (g water/g dried nanocomposite) was calculated using Eq. (1):

$$\mathrm{DS(g/g)} = \frac{W_\mathrm{s} - W_\mathrm{d}}{W_\mathrm{d}} \tag{1}$$

where W_s and W_d are the weights of the swollen nanocomposites and the dry sample, respectively. Absorbency of the nanocomposite hydrogels was evaluated in 0.15 M solutions of NaCl, $CaCl_2$, and KCl as similar to distilled water.

To investigate the effect of pH on the degree of swelling of hydrogels, the 0.1 g of samples were immersed into 50 mL of non-buffered solutions (prepared by dilution of HCl or NaOH solutions) or buffered solutions with the concentration of 0.2 M. The degree of swelling was measured as above.

Adsorption studies

Adsorption experiments were done at ambient temperature by immersing of 0.05 g of samples into 50 mL of dye solution with 50 ppm concentration. The flasks containing samples in the dye solution were placed on a shaker with 120 rpm. To study the adsorption kinetics, at specified time intervals, the amount of adsorbed CV was evaluated using a UV spectrometer at $\lambda_{\max} = 590$ nm. The content of adsorbed dye was calculated using the following Eq. 2:

$$q_t = \frac{(C_0 - C_t)}{m} \times V \tag{2}$$

where C_0 is the initial CV concentration (mg L^{-1}), C_t is the remaining dye concentrations in the solution at time t, V is the volume of dye solution used (L), and m is the weight of nanocomposite (g). Adsorption isotherm was carried out by immersing of 0.05 g of nanocomposites into 50 mL of dye solutions with 20, 30, 40, 50, 60, 70, and 80 mg L^{-1} of CV for 24 h. The equilibrium adsorption capacity of nanocomposites, q_e (mg g^{-1}), was determined using Eq. 2. At this equation, the C_t and the q_t will be replaced with equilibrium concentration of dye in the solution (C_e) and equilibrium adsorption capacity (q_e), respectively.

To study the effect of pH of initial dye solution on the adsorption, the pH of water was adjusted to desired pH using 0.1 M of HCl and NaOH solutions and the 50 mg L^{-1} of CV dye was prepared at the obtained pHs.

For desorption study, the sample containing adsorbed dye was immersed into 50 mL of desorption solution at ambient temperature for 5 h. The desorption solution was prepared from dissolving of KCl in ethanol/water mixture (50/50 V/V). The concentration of KCl was changed from 0 to 0.45 M. Desorption content was measured using spectrophotometer and according to calibration curves for each desorption solution.

Characterization

Dried nanocomposite was coated with a thin layer of gold and imaged in a SEM instrument (Vega, Tescan). TEM micrographs were recorded with a Philips CM10 operating at 60 kV tension. A thermal analyzer (Mettler Toledo) was used for thermogravimetric analysis (TGA) under nitrogen. The heating rate was 20 °C/min. The FTIR spectra were performed using Bruker Tensor 27 spectrophotometer (KBr pellets).

Results and discussion

Synthesis and characterization

Nanocomposite hydrogels were prepared by graft copolymerization of AAm onto *kappa*-carrageenan backbones using the MBA cross-linker and the sepiolite nanoclay. APS was used as initiator. The persulfate initiator can decompose under heating and the resultant radicals will induce free radicals onto *kappa*-carrageenan. AAm monomer can graft onto carrageenan through produced radicals. In the presence of a cross-linker, i.e., MBA, cross-linking reaction can occur and finally a three-dimensional network is produced. The sepiolite nanoclays can capture in the produced nanocomposite network. A simple scheme for synthesis of nanocomposite hydrogel was shown in Fig. 1.

The FTIR of neat sepiolite is illustrated in Fig. 2a. The bands at 3,564–3,700 cm^{-1} are attributed to the OH groups in the octahedral sheet and the OH stretching vibration at the external surface of sepiolite. The band at 1,660 cm^{-1} is due to the OH stretching of bound water coordinated to magnesium in the octahedral sheet. The bands at 1,211 and 1,018 cm^{-1} represent the stretching of Si–O in the Si–O–Si groups of the tetrahedral sheet. The FTIR of H sample (Fig. 2b) showed bands at 846, 927, 1,038, and 1,252 cm^{-1} that can be attributed to D-galactose-4-sulfate, 3,6-anhydro-D-galactose, glycosidic linkage, and ester sulfate stretching of carrageenan, respectively. The presence of polyacrylamide was confirmed by the peaks at 1,648 cm^{-1} (C=O stretching) and 3,200 cm^{-1} ($–NH_2$ stretching). In the NH10 spectrum (Fig. 2b), the bands of sepiolite at 3,564–3,700 cm^{-1} disappeared that can be attributed to the interaction of OH

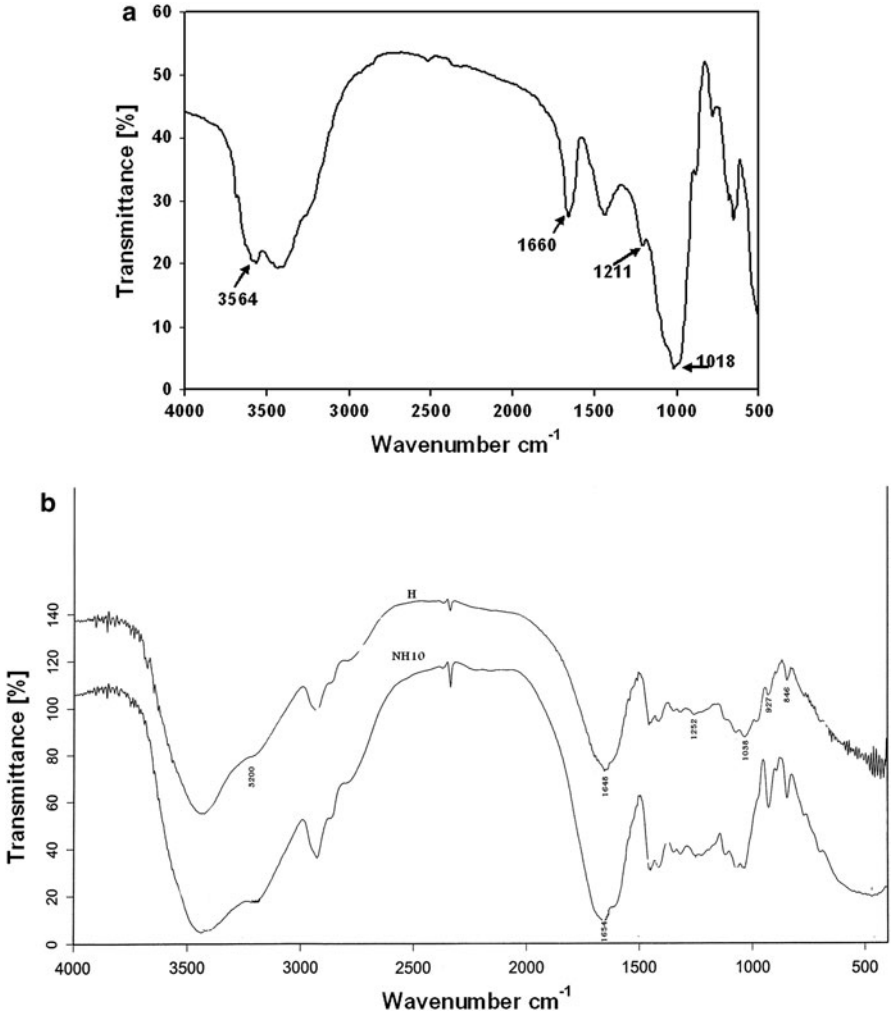

Fig. 2 FTIR of **a** neat sepiolite and **b** clay-free hydrogel and NH10 hydrogel

groups of sepiolite with functional groups of hydrogel. This interaction may be confirmed from shifting of C=O stretching band from 1,648 to 1,654 cm^{-1}.

The morphology of nanocomposite was investigated using TEM image. The sepiolite clay was used without any chemical treatment. It has been reported that the sepiolite can themselves aggregate to form bundle of needles [27]. According to Fig. 3a, the sepiolite nanoparticles exist as individual needles. The uniform dispersion of sepiolite can be attributed to ultrasonic treatment as well as polymerization of acrylamide that can stabilize the dispersed needles of sepiolite particles. One of the most crucial properties of nanocomposites which can be considered is hydrogel microstructure morphology. Figure 3b, c shows the SEM micrographs of clay-free hydrogel and nanocomposite containing 5 wt% of

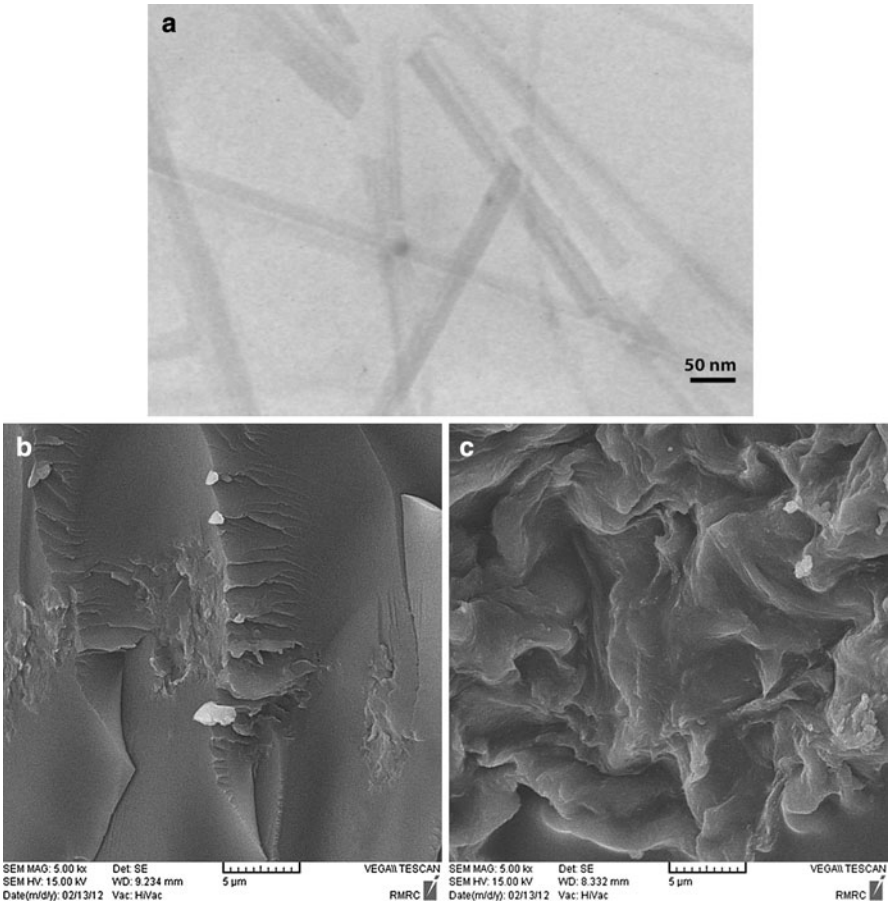

Fig. 3 **a** TEM image of nanocomposite containing 5 wt% of sepiolite (NH5), and SEM images of clay-free hydrogel (**b**) and NH5 nanocomposite hydrogel (**c**)

nanoclay. While the hydrogel without clay shows a relatively tight and smooth surface (Fig. 3b), the nanocomposite (Fig. 3c) contains coarse and undulant surface.

The effect of sepiolite on the thermal stability of hydrogels was studied and the results are illustrated in Fig. 4a–c. It has been reported that by introducing of clay into polymeric matrix, the thermal stability of product can be improved [28]. According to the TGAs graphs of hydrogels, three stages of decomposition can be seen from the samples. The first is in the range from 50 to 230 °C. This weight loosing can be attributed to the moisture in the samples. The values of weight loss for clay-free hydrogel, NH5, and NH10 are 1.81, 1.97, and 1.51 wt%, respectively. The second stage is range from 250 to 350 °C that attribute to decomposition of amide groups of PAAm chains and carrageenan backbones. At this stage, the values of weight loss for clay-free hydrogel, NH5, and NH10 are 18.6, 17.8, and 16.5 wt%, respectively. The introducing of sepiolite caused an improvement in thermal stability of hydrogel. In the third stage, ranging from 350 to 480 °C, the weight loss

for clay-free hydrogel, NH5, and NH10 are 58.2, 51.9, and 48.2 wt%, respectively. These observations confirm the increase of thermal stability of hydrogels by introducing sepiolite clay. As a comparative graph, Fig. 4d shows the difference in thermal stability of products.

Swelling studies

The swelling of hydrogel and nanocomposite hydrogels as a function of salinity and pH of media was investigated. The degree of swelling of hydrogels in distilled water and 0.15 M of salt solutions was shown in Fig. 5. As can be seen from figure, by inclusion of sepiolite nanoclay, swelling capacity of carrageenan-based hydrogels was decreased. This reduction in water absorbency can be attributed to the increase in cross-linking points from the formation of hydrogen bonding between silanol groups (–SiOH) on the surface of sepiolite and amide (from polyacrylamide chains) or hydroxyl (from carrageenan chains) groups [29]. Since the carrageenan-based nanocomposite hydrogels are comprised sulfate groups, they exhibited various swelling capacity in different salt solutions with same concentrations. These swelling changes are due to valency difference of salts. The swelling capacity decreased with an increase in charge of the metal cation ($Ca^{2+} < Na^{+}$). It may be explained by complexing ability arising from the coordination of the multivalent cations with sulfate groups on carrageenan backbones [30]. But when the hydrogels were swollen in K^{+} solution, the swelling capacity was obtained lower than the Ca^{2+} and Na^{+} solutions. This can be attributed to the high tendency of sulfate groups on the carrageenan to complex with K^{+} cations than that of Ca^{2+} [31].

To investigate the effect of pH on the swelling capacity, first the equilibrium swelling (ultimate absorbency) of the hydrogels was studied at various pHs ranged from 2.0 to 12.0 (Fig. 6). No additional ions (through buffer solution) were added to medium for setting pH because absorbency of a hydrogels is strongly affected by ionic strength [32]. Therefore, stock NaOH (pH 12.0) and HCl (pH 2.0) solutions were diluted with distilled water to reach desired basic and acidic pHs, respectively. According to Fig. 6a, the swelling capacity of hydrogels was about constant from pH 4 to 10. A slightly change in degree of swelling was observed at pH 2 and 12. At these pHs, a screening effect of the counter ions, i.e., H^{+} at pH 2 and Na^{+} at pH 12, shields the charge of the sulfate anions and prevents an efficient repulsion [33]. However, the degree of swelling of hydrogels in buffered solutions was obtained lower than non-buffered solutions (Fig. 6b). This is due to higher ionic strength of the buffer solutions. But the swelling values were not remarkably changed by varying the pH of solutions. The carrageenan-based hydrogels in this study comprise *kappa*-carrageenan, polyacrylamide, and sepiolite components. Among them, polyacrylamide and sepiolite are non-ionic and pH-independent. *kappa*-Carrageenan is an ionic polysaccharide comprising sulfate groups ($–OSO_3^-$). These pendants are completely dissociated in the overall pH range and the hydrogels from this biopolymer shows pH-independent swelling behavior [34]. In fact, in the overall pH range, these anionic groups are in dissociation form, and the similar swelling values at various buffered pHs can be attributed to this property of carrageenan.

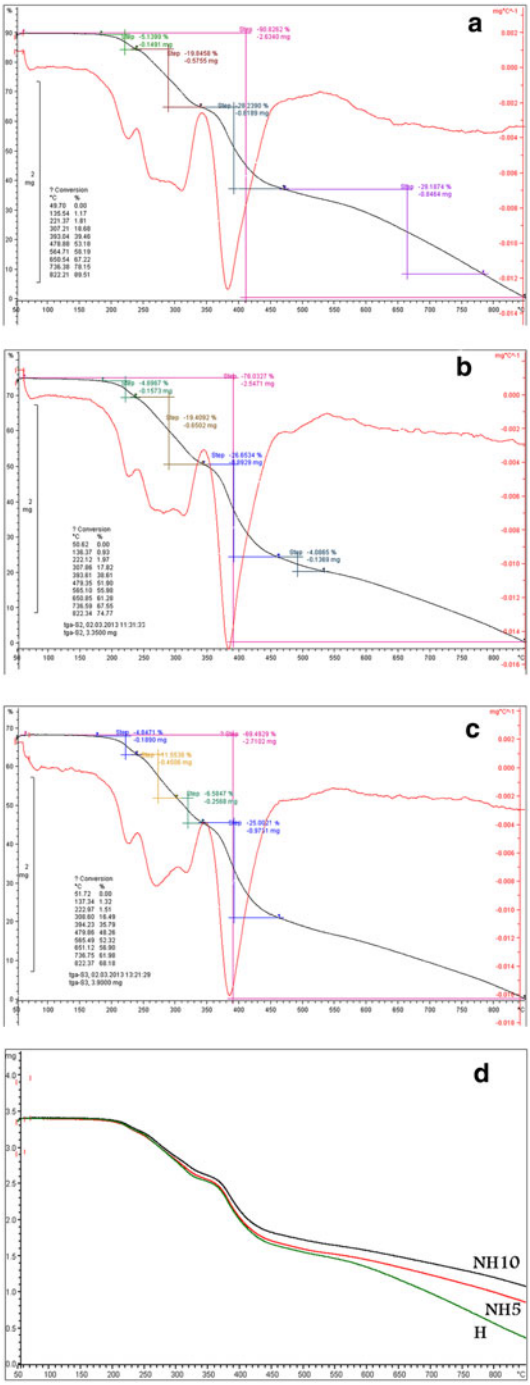

Fig. 4 TGAs graphs of **a** clay-free, **b** NH5, **c** NH10, and **d** their comparison

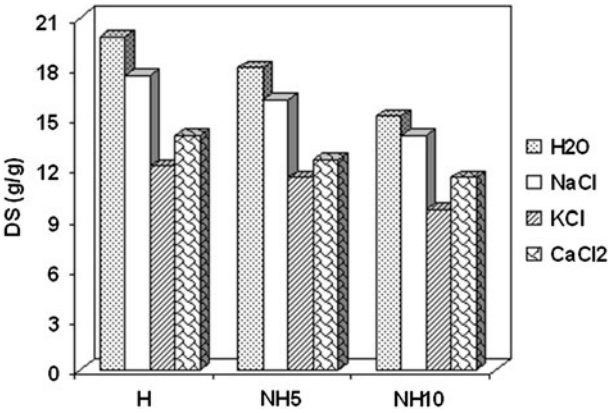

Fig. 5 Swelling of hydrogels in distilled water and salt solutions with 0.15 M

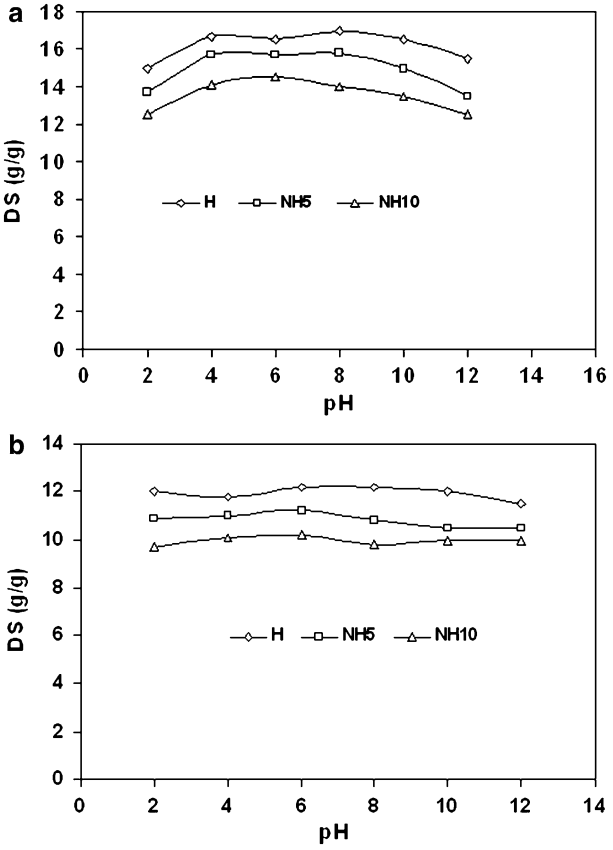

Fig. 6 Effect of pH on the swelling of hydrogels in **a** non-buffered solutions and **b** buffered solutions

Dye adsorption Study

Kinetic of adsorption

Adsorption kinetic as a useful information on the rate of dye adsorption can be consider as an important factor to properly design adsorbent [35]. So, the adsorption kinetic was investigated to measure the required equilibrium time of adsorption on samples. The adsorption of CV dye on the samples was examined for 5 h and the results are depicted in Fig. 7a. Initially, the adsorption of dye onto hydrogels sharply increases and then begins to level off. The equilibrium dye adsorption was achieved after ~3 h. It is clear from figure that by introducing sepiolite clay in carrageenan-based hydrogels, the dye adsorption capacity gets increased. Furthermore, from the initial slope of the curves, the speed of dye adsorption is enhanced as the clay amount is increased in hydrogel composition. Although the water absorbency of nanocomposites was decreased by introducing the sepiolite nanoclay, the increment in both dye adsorption capacity and rate can be attributed to increase the adsorbing centers in hydrogel composition. A similar observation was obtained in our previous work using sodium montmorillonite nanoclay [25]. For comparison, the dye adsorption onto neat sepiolite was examined and show in Fig. 7a. The dye adsorption speed and capacity for neat clay are higher than the hydrogels. The high rate of adsorption and capacity can be attributed to the more adsorption center as well as the fine size of particles. But it may be noted that although the dye adsorption speed and capacity of neat clay were high, but due to the small size of clay, more time was needed to settle in solution.

Pseudo-first-order, pseudo-second-order, and intraparticle diffusion kinetic models were examined to obtain rate constant and equilibrium adsorption capacity for hydrogel samples. Kinetic data were analyzed using the pseudo-first-order equation as below [36]:

$$\log(q_e - q_t) = \log q_{e1} - \frac{k_1}{2.3} t \tag{3}$$

where q_e and q_t (mg g^{-1}) are the amount of adsorbed dye on the nanocomposites at equilibrium and at time t, respectively. k_1 (min^{-1}) presents the rate constant of first-order adsorption. q_{e1} indicates the theoretically equilibrium adsorption. In order to obtain model calculations k_1, q_{e1}, and R^2 (correlation coefficient), we can plot $log(q_e - q_t)$ against t for pseudo-first-order.

Also, kinetic data were analyzed using the pseudo-second-order equation as below [36]:

$$\frac{t}{q_t} = \frac{1}{k_2 q_{e2}^2} + \frac{t}{q_{e2}} \tag{4}$$

here k_2 (g mg^{-1} min^{-1}) is rate constant of second-order adsorption, and q_{e2} is the theoretical adsorbed dye (mg g^{-1}) that can be calculated from pseudo-second-order. In order to obtain model calculations k_2 and theoretically equilibrium adsorption (q_{e2}) as well as R^2 (correlation coefficient), we can plot $\frac{t}{q_t}$ against t (Fig. 7b). Model

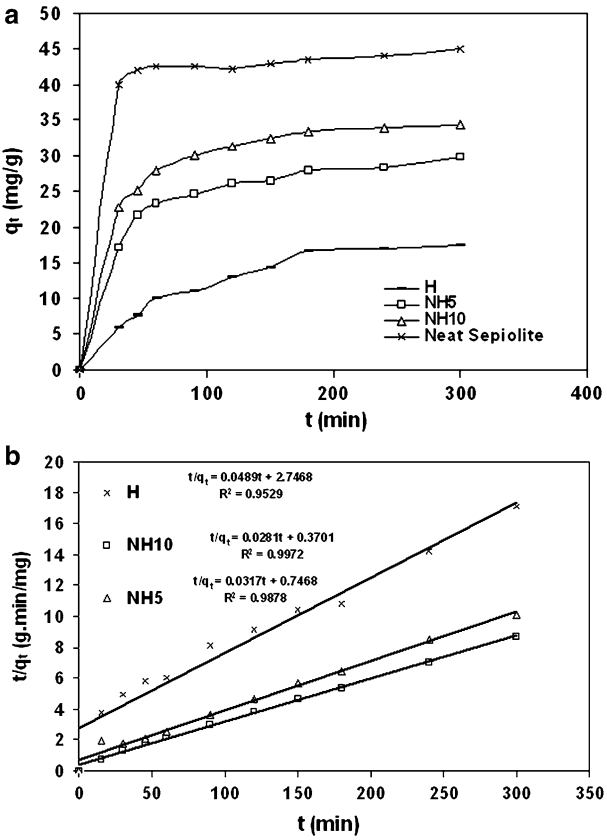

Fig. 7 Adsorption content of dye by samples as a function of contact time (**a**). Adsorption kinetic of the CV onto hydrogel and hydrogel nanocomposites according to pseudo-second-order model (**b**). (0.05 g of hydrogels, 50 mL of CV dye with 50 ppm concentration, 120 rpm, $T = 25$ °C)

calculations for all nanocomposites were given in Table 1. It was found that the plotting of $\frac{t}{q_t}$ against t gives a straight-line with a high correlation coefficient ($R^2 > 0.95$), and it can be concluded that adsorption kinetic of dye by all nanocomposites has the best fitting to the pseudo-second-order. As can be seen from the data, according to pseudo-second-order kinetic, the theoretical equilibrium adsorption capacities are in agreement with the experimental data.

The adsorption of adsorbate to the adsorbent can take place through several steps. The steps may be considered as film diffusion, pore diffusion, surface diffusion, and adsorption on the pore surface [37]. In fact, under sufficient speed of stirring, intraparticle diffusion/transport process is the rate-limiting steps of adsorption kinetic [37]. The possibility of intraparticle diffusion can explore according to Eq. 5:

Table 1 The pseudo-first-order and pseudo-second-order rate parameters for CV adsorption onto nanocomposites

	First-order kinetics				Second-order kinetics		
	q_{e1}, mg g^{-1}	q_e, Exp., mg g^{-1}	$k_1 \times 10^3$, min^{-1}	R^2	q_{e2}, mg g^{-1}	$k_2 \times 10^3$, g mg^{-1} min^{-1}	R^2
H	33.1	20.4	0.39	0.8853	20.4	0.87	0.9529
NH5	30.9	29.8	1.6	0.7873	31.5	1.34	0.9878
NH10	17.8	34.4	1.6	0.8786	35.6	2.13	0.9972

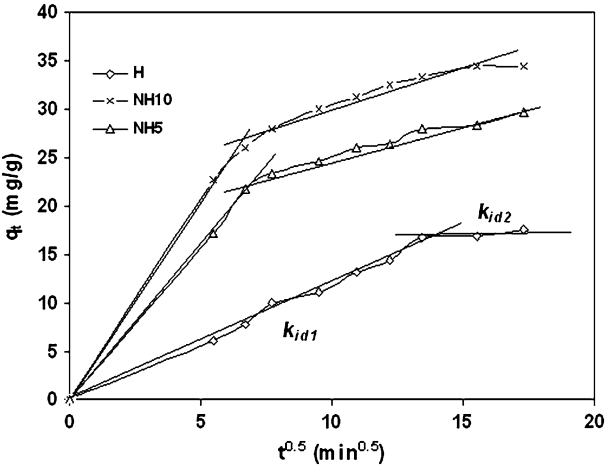

Fig. 8 Intraparticle diffusion kinetics of CV dye adsorption onto nanocomposites

$$q_t = k_{\mathrm{id}} t^{0.5} + C \tag{5}$$

where q_t is the amount of dye adsorbed at time t, C is the intercept, and k_{id} is the intraparticle diffusion rate constant (mg $min^{0.5}$ g^{-1}).

According to Eq. 5, by plotting q_t versus $t^{0.5}$, a straight-line suggests that the intraparticle diffusion is the rate-limiting step. As seen from Fig. 8, the diffusion plot of CV onto nanocomposites is multi-linear containing two linear parts. The linear segments did not pass through the origin, indicating that the intraparticle diffusion is not the only rate-limiting step. The first linear segments show that the mass transfer controlling may be due to boundary layer effect [38]. Slops of two linear segments are not similar and the first segment comprises sharper slop. The separate intraparticle diffusion parameters for two sections are summarized in Table 2. As seen from data, the k_{id1} value is enhanced as the sepiolite is increased in hydrogel composition indicating improvement of the rate of adsorption by hydrogel nanocomposites. Also, the k_{id} values for second linear sections are smaller than first segments, and this observation shows that the rate of dye adsorption at first section

Table 2 The k_{id} and correlation coefficient parameters according to intraparticle diffusion model for linear sections

	Intraparticle diffusion model			
	k_{id1}	R_1^2	k_{id2}	R_2^2
H	1.22	0.9928	1.07	0.9729
NH5	3.2	0.9992	1.65	0.8446
NH10	3.96	0.9969	1.95	0.8255

occurs faster than the second section. The high speed of adsorption at first part can be attributed to ease of availability of adsorption centers [38].

Adsorption isotherm

Adsorption isotherm can be considered as an essential necessity to design adsorption system. In the adsorption isotherm studies, the hydrogels were immersed into dye solutions with different initial concentration ranging from 20 to 80 mg/L. The adsorption capacity of hydrogels was calculated at equilibrium time. Figure 9a shows the effect of initial dye concentration on the adsorption capacity of hydrogels. As the initial dye concentration is increased, the adsorption capacity of samples is enhanced and then switches to level off. At higher initial concentration, the adsorption sites reach on saturation state and the adsorption remains constant. The Langmuir and Freundlich isotherm models can be applied to analyze experimentally equilibrium data from adsorption of dye onto samples at equilibrium time.

In the Langmuir adsorption model, adsorption of adsorbate takes place at specific homogeneous sites within the adsorbent and valid for monolayer adsorption onto adsorbents [39]. The expression of the applied Langmuir model is given by the Eq. 6:

$$\frac{C_e}{q_e} = \frac{C_e}{q_m} + \frac{1}{q_m b} \tag{6}$$

where C_e is the equilibrium dye concentration in the solution (mg/L), b is the Langmuir adsorption constant (L/mg), and q_m is the theoretical maximum adsorption capacity (mg g^{-1}). The q_m and b can be calculated from the slope and intercept of a linear plot of $\frac{C_e}{q_e}$ versus C_e, respectively (Fig. 9b).

In the Freundlich model, the adsorption of adsorbate occurs on a heterogeneous surface by multilayer sorption, and the adsorption capacity increases with an increase in adsorbate concentration [39]. Freundlich isotherm is represented by the following equation:

$$\log q_e = \log k_f + \frac{1}{n} \log C_e \tag{7}$$

where k_f is the equilibrium adsorption coefficient (L/g) and *1/n* is the empirical constant. The k_f and n values for nanocomposites can be achieved from the intercept and the slop of plotting $\log q_e$ against $\log C_e$, respectively. In fact, the n value depicts the favorability of adsorption process and k_f is the adsorption capacity and intensity of the adsorbate.

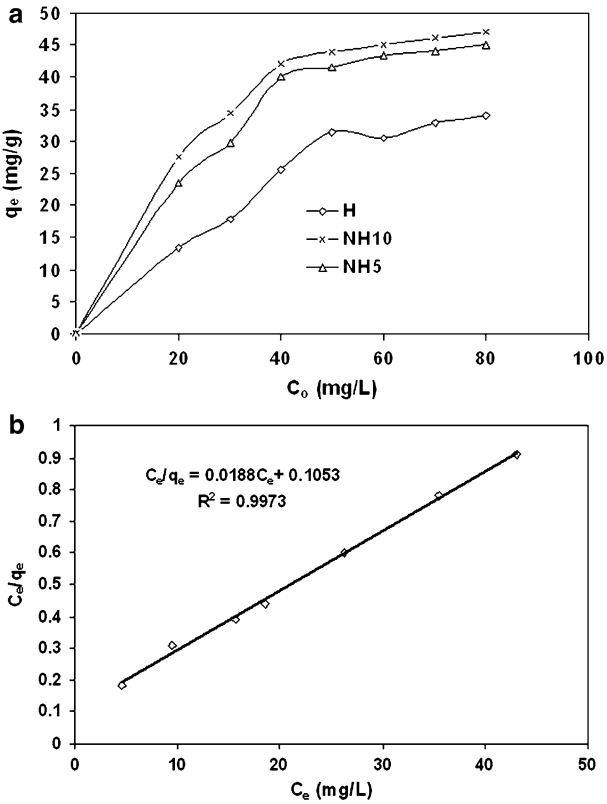

Fig. 9 Effect of initial dye concentration on the equilibrium dye adsorption capacity (**a**) and plot of C_e/q_e versus C_e according to Langmuir isotherm (**b**)

All expressions in Langmuir and Freundlich equations and equilibrated adsorption of all nanocomposites were calculated according to experimental data and summarized in Table 3. In accordance with the high correlation coefficient in Langmuir equation ($R^2 > 0.97$), it depicts that Langmuir isotherm is the best fit for experimental data than the Freundlich model. From Langmuir parameters, the theoretical and experimental maximum adsorption capacities of hydrogels are in agreement and confirming the best fit of Langmuir model with practical data. The favorability of the adsorption (R_L) was evaluated from parameters of Langmuir adsorption isotherm model. The R_L can calculate from the following equation [40]:

$$R_L = \frac{1}{1 + bC_0} \tag{8}$$

where b is the Langmuir constant (L/mg) and C_0 is the initial concentration of dye. The R_L can vary: for $R_L > 1$, the adsorption is unfavorable; $R_L = 1$, the adsorption is linear condition; the adsorption is favorable when $0 < R_L < 1$; and $R_L = 0$ is for irreversible conditions. According to Table 3, the R_L values for hydrogels were

Table 3 Isotherm parameters for adsorption of CV onto nanocomposites

Isotherm	Parameters	Samples		
		H	NH5	NH10
Freundlich model	n, g L^{-1}	9.2	5.3	4
	k_f, mg g^{-1}	21.7	19.9	17.7
	R^2	0.8169	0.712	0.8436
Langmuir model	q_m, mg g^{-1}	34.3	49.5	53.2
	b, L mg^{-1}	0.012	0.0034	0.0033
	R^2	0.9942	0.9776	0.9973
	R_L	0.73	0.9	0.91
q_e (q_m exp), mg g^{-1}		34	45	47

achieved between one and zero indicating favorable adsorption of CV onto obtained hydrogel nanocomposites.

Effect of pH on adsorption

The pH of adsorption media can affect the adsorption of adsorbate onto adsorbent. So, to investigate the influence of pH of dye solution on the removal efficiency, the adsorption experiments were examined at pH 2–10. The results are illustrated in Fig. 10a. The H sample comprises *kappa*-carrageenan and polyacrylamide components. While the PAAm chains contain non-ionic and pH-independent amide groups, *kappa*-carrageenan is an ionic polysaccharide comprising sulfate groups ($-OSO_3^-$). These pendants are completely dissociated in the overall pH range, and the hydrogels from this biopolymer shows pH-independent swelling behavior [34]. In fact, in the overall pH range, these anionic groups are in dissociation form. As it evident from Fig. 10a that, by varying the pH of initial dye solution, the change in dye adsorption of H samples is not notable and can be attributed to complete dissociation of anionic groups on *kappa*-carrageenan at overall pH range. But the hydrogels containing sepiolite nanoclay showed pH-dependent dye adsorption capacity. While the adsorption capacity of nanocomposites was not considerable up to pH 6, at basic solutions, the dye adsorption capacity of hydrogels containing sepiolite was enhanced. This increment can be attributed to the increase of negative centers on sepiolite in the presence of excess hydroxyl groups. Similar observation has been reported by Dogan et al. using sepiolite clay to remove cationic dye [38]. The dye adsorption capacity of clay-free hydrogel is in agreement with swelling data in buffered solutions. In spite of similar swelling behavior of nanocomposites and clay-free hydrogel, an increase in dye adsorption capacity was observed at high pHs.

The influence of pH on the rate of dye removal of NH10 hydrogel was illustrated in Fig. 10b. The initial slopes of plots depicts that the pH of initial dye solution can affect the rate of dye removal by sample. The speed of dye removal at acidic pH is lower than basic media. It may be attributed to compete dye cation and H^+ for active center of adsorption.

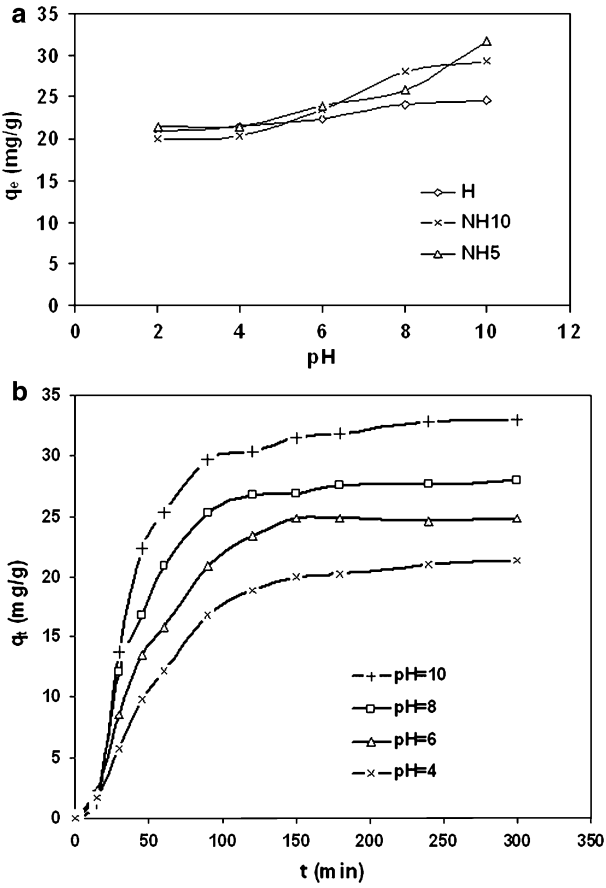

Fig. 10 Effect of pH on the dye adsorption capacity of hydrogels (**a**) and effect of pH on the dye adsorption speed of NH10 nanocomposite (**b**)

The maximum dye adsorption capacity of carrageenan-based nanocomposite at this study and some other adsorbents is compared in Table 4. The results indicate that the adsorption capacity of carrageenan-based nanocomposite is comparable with other adsorbents.

Adsorption–desorption studies

To evaluate the possibility of reusing of nanocomposite hydrogels over multiple cycles, desorption–adsorption process of dye by nanocomposites was examined using KCl solutions in water/ethanol mixture. When the ethanol/water solution was used as desorption solution, desorption content was obtained low. By introducing the KCl in desorption solution, desorption yield was improved. But by increasing the KCl concentration from 0.15 to 0.45 M, the desorption content was not changed considerably. So, the 0.15 M of KCl solution in water/ethanol mixture was used to

Table 4 Maximum adsorption capacities of CV dye onto some adsorbent and *kappa*-carrageenan-based nanocomposite hydrogels

Adsorbent	Maximum dye adsorption, mg g^{-1}	Reference
Wollastonite	8.8	[41]
Semi-IPN hydrogel	35	[42]
Magnetic nanocomposite	81.7	[43]
Bagasse fly ash	26.2	[44]
Raw Kaolin	44.8	[45]
[a]Carra-Na-MMt	42.8	[25]
[b]Carra-Laponite	67	[24]
NH10	47	This study

[a] Carrageenan-poly(acrylamide)-sodium montmorillonite nanocomposite containing about ~10 wt of sodium montmorillonite

[b] Carrageenan-poly(acrylamide)-laponite RD nanocomposite containing about ~10 wt of laponite RD

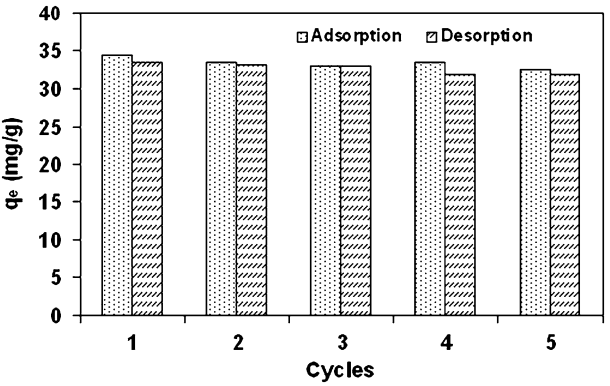

Fig. 11 Adsorption and desorption behavior of CV dye onto NH10 nanocomposite

desorption of dye from NH10 sample. The adsorption–desorption process was repeated for five times. The results are illustrated in Fig. 11. As it is clear from figure, the adsorption capacity and desorption content during five cycles was not changed considerably. Because of high recycling efficiency, the present nanocomposite can be considered as adsorbent for practical applications.

Conclusion

In the present work, *kappa*-carrageenan-based nanocomposites containing sepiolite nanoclay were synthesized, and the TEM image revealed that sepiolite nanoclay exists as individual needles. The adsorption of cationic CV dye onto obtained hydrogels was improved by introducing sepiolite nanoclay. The presence of sepiolite in hydrogel composition caused an enhancement in adsorption capacity and speed of dye removal. The results showed that the pseudo-second-order adsorption kinetic was predominated for the adsorption of CV onto hydrogels. Langmuir model was obtained as the best model for the adsorption of CV onto

nanocomposites. Studying the pH of initial dye solutions on the dye adsorption of hydrogels depicted that while the clay-free hydrogel shows relatively pH-independent behavior, the nanocomposites adsorbed high content dye at basic media. Also, at basic condition, the rate of dye adsorption obtained was higher than acidic media.

Acknowledgments The authors would like to specially thank the referees for their good suggestions for improving the manuscript.

References

1. Omidian H, Rocca JG, Park K (2005) Advances in super-porous hydrogels. J Control Release 102:3
2. Chang C, Zhang L (2011) Cellulose-based hydrogels: present status and application prospects. Carbohyd Polym 84:40
3. Mahdavinia GR, Pourjavadi A, Zohuriaan-Mehr MJ (2006) A convenient one-step preparation of chitosan-poly(sodium acrylate-*co*-acrylamide) hydrogel hybrids with super-swelling properties. J Appl Polym Sci 99:1615
4. Wang Q, Wang W, Wu J, Wang A (2012) Effect of attapulgite contents on release behaviors of a pH sensitive carboxymethyl cellulose-*g*-poly(acrylic acid)/attapulgite/sodium alginate composite hydrogel bead containing diclofenac. J Appl Polym Sci 24:4424
5. Hosseinzadeh H, Pourjavadi A, Mahdavinia GR, Zohuriaan-Mehr MJ (2005) Modified Carrageenan. 1. H-CarragPAM, a Novel Biopolymer-Based Superabsorbent Hydrogel. J Bioact Compat Pol 20:475
6. Gad YH, Aly RO, Abdel-Al SE (2011) Synthesis and characterization of Na-alginate/acrylamide hydrogel and its application in dye removal. J Appl Polym Sci 120:1899
7. Lin H, Dan W, Dan N (2012) The water state in crosslinked poly(vinyl alcohol)–collagen hydrogel and its swelling behavior. J Appl Polym Sci 123:2753
8. Hu X (2011) Synthesis and properties of silk sericin-*g*-poly(acrylic acid-co-acrylamide) superabsorbent hydrogel. Polym Bull 66:447
9. Pourjavadi A, Barzegar Sh, Mahdavinia GR (2006) MBA-crosslinked Na-Alg/CMC as a smart full-polysaccharide superabsorbent hydrogels. Carbohyd Polym 66:386
10. Nair LS, Laurencin CT (2007) Biodegradable polymers as biomaterials. Prog Polym Sci 32:762
11. Zainal Z, Hui LK, Hussein MZ, Abdullah AH, Hamadneh IR (2009) Characterization of TiO_2–Chitosan/Glass photocatalyst for the removal of a monoazo dye via photodegradation–adsorption process. J Hazard Mater 164:138
12. Cirini G (2005) Non-conventional low-cost adsorbents for dye removal: a review. Bioresource Technol 97:1061
13. Hamidi M, Azadi A, Rafiei P (2008) Hydrogel nanoparticles in drug delivery. Adv Drug Deliv Rev 60:1638
14. Jiuhui Q (2008) Research progress of novel adsorption processes in water purification: a review. J Environ Sci 20:1
15. Liu P, Zhang L (2007) Adsorption of dyes from aqueous solutions or suspensions with clay nano-adsorbents. Sep Purif Technol 58:32
16. Dalaran M, Emik S, Guclu G, Iyim TB, Ozgumus S (2009) Removal of acidic dye from aqueous solutions using poly(DMAEMA–AMPS–HEMA) terpolymer/MMT nanocomposite hydrogels. Polym Bull 63:159
17. Li PS, Kim NH, Yoo GH, Lee JH (2009) Poly(acrylamide/laponite) nanocomposite hydrogels: swelling and cationic dye adsorption properties. J Appl Polym Sci 111:1786
18. Kaplan M, Kasgoz H (2011) Hydrogel nanocomposite sorbent for removal of basic dye. Polym Bull 67:1153
19. Ekici S, Isikver Y, Saraydın D (2006) Poly(acrylamide-sepiolite) composite hydrogels: preparation, swelling and dye adsorption properties. Polym Bull 57:231
20. Shirsath SR, Hage AP, Zhou M, Sonawane SH, Ashokkumar M (2011) Ultrasound assisted preparation of nanoclay Bentonite-FeCo nanocomposite hybrid hydrogel: a potential responsive sorbent for removal of organic pollutant from water. Desalination 281:429

21. Takemasa M, Chiba A, Date M (2001) Gelation mechanism of κ- and ι-carrageenan investigated by correlation between the strain-optical coefficient and the dynamic shear modulus. Macromolecules 34:7427
22. Antonov YA, Goncalves MP (1999) Phase separation in aqueous gelatin-kappa-carrageenan systems. Food Hydrocoll 13:517
23. Mansfeld J, Dautzenberg H (1997) Immobilization of cells in polyelectrolyte complexes. Method Biotechnol 1:309
24. Mahdavinia GR, Massoudi A, Baghban A, Massoumi B (2012) Novel carrageenan-based hydrogel nanocomposites containing laponite RD and their application to remove cationic dye. Iran Polym J 21:609
25. Mahdavinia GR, Massoumi B, Jalili K, Kiani GR (2012) Effect of sodium montmorillonite nanoclay on the water absorbency and cationic dye removal of carrageenan-based nanocomposite superabsorbents. J Polym Res 19:9947
26. Mahdavinia GR, Zhalebaghy R (2012) Removal kinetic of cationic dye using poly (sodium acrylate)-carrageenan/Na-montmorillonite nanocomposite superabsorbents. J Mater Environ Sci 3:895
27. Yu Y, Qi S, Zhan J, Wu Z, Yang X, Wu D (2011) Polyimide/sepiolite nanocomposite films: preparation, morphology and properties. Mater Res Bull 46:1593
28. Sur GS, Lyu SG, Chang JH (2003) Synthesis and LCST behavior of thermosensitive poly(N-isopropylacrylamide)-clay nanocomposites. J Ind Eng Chem 9:58
29. Alkan M, Benlikaya R (2009) Poly(vinyl alcohol) nanocomposites with sepiolite and heattreated sepiolites. J Appl Polym Sci 112:3764
30. Mahdavinia GR, Zohuriaan-Mehr MJ, Pourjavadi A (2004) Modified chitosan III, superabsorbency, salt- and pH-sensitivity of smart ampholytic hydrogels from chitosan-g-PAN. Polym Adv Technol 15:173
31. Mohamadnia Z, Zohuriaan-Mehr MJ, Kabiri K, Jamshidi A, Mobedi H (2007) pH-sensitive IPN hydrogel beads of carrageenan-alginate for controlled drug delivery. J Bioact Compat Pol 22:342
32. Flory PJ (ed) (1953) Principles of polymer chemistry. Cornell University Press, Ithaca
33. Mahdavinia GR, Pourjavadi A, Hosseinzadeh H, Zohuriaan-Mehr MJ (2004) Modified chitosan 4. Superabsorbent hydrogels from poly(acrylic acid-co-acrylamide) grafted chitosan with salt- and pH-responsiveness properties. Eur Polym J 40:1399
34. Durmaz S, Okay O (2000) Acrylamide/2-acrylamido-2-methylpropane sulfonic acid sodium salt-based hydrogels: synthesis and characterization. Polymer 41:3693
35. Liu B, Lv X, Wang D, Xu Y, Zhang L, Li Y (2012) Adsorption behavior of As(III) onto chitosan resin with As(III) as template ions. J Appl Polym Sci 125:246
36. Auta M, Hameed BH (2011) Preparation of waste tea activated carbon using potassium acetate as an activating agent for adsorption of Acid Blue 25 dye. Chem Eng J 171:502
37. Ho YS, McKay G (2003) Sorption of dyes and copper ions onto biosorbents. Process Biochem 38:1047
38. Alkan M, Demirbas O, Dogan M (2007) Adsorption kinetics and thermodynamics of an anionic dye onto sepiolite. Micropor Mesopor Mater 101:388
39. Singh KP, Mohan D, Sinha S, Tondon GS, Gosh D (2003) Color removal from wastewater using low-cost activated carbon derived from agricultural waste material. Ind Eng Chem Res 42:1965
40. Zhu HY, Fu YQ, Jiang R, Yao J, Xiao L, Zeng GM (2012) Novel magnetic chitosan/poly(vinyl alcohol) hydrogel beads: preparation, characterization and application for adsorption of dye from aqueous solution. Bioresource Technol 105:24
41. Khare SK, Srivastavar RM, Panday KK, Singh VN (1988) Removal of basic dye (crystal violet) from water using wollastonite as adsorbent. Environ Technol Lett 9:1163
42. Li S (2010) Removal of crystal violet from aqueous solution by sorption into semi-interpenetrated networks hydrogels constituted of poly(acrylic acid-acrylamide-methacrylate) and amylase. Bioresource Technol 101:2197
43. Singh KP, Gupta S, Singh AK, Sinha S (2011) Optimizing adsorption of crystal violet dye from water by magnetic nanocomposite using response surface modeling approach. J Hazard Mater 186:1462
44. Mall ID, Srivastava VC, Agarwal NK (2006) Removal of Orange-G and Methyl Violet dyes by adsorption onto bagasse fly ash—kinetic study and equilibrium isotherm analyses. Dyes Pigments 69:210
45. Nandi BK, Goswami A, Das AK, Mondal B, Purkait MK (2008) Kinetic and equilibrium studies on the adsorption of crystal violet dye using kaolin as an adsorbent. Sep Sci Technol 43:1382